ORIGINAL CONTRIBUTION

CrossMark

The influence of zinc gluconate as an intercalating agent on the structural, thermal, morphologic, and molecular mobility of lamellar nanofiller

Ana L. F. Carvalho[1] · Daniela F. S. Freitas[1] · Danielle M. Mariano[1] · Gabriela C. Mattos[1] · Luis C. Mendes[1]

Abstract

The purpose of this work was to investigate the influence of zinc gluconate (ZnG) as an intercalating agent on the properties of lamellar zirconium phosphate (α-ZrP). This nanofiller was synthesized by direct precipitation and it was evaluated as a host for zinc gluconate. Structural, thermal, morphology, and molecular mobility characteristics were assessed. Infrared spectroscopy (FTIR) evidenced that the ZrP and ZnG strongly interacted to each other. Wide-angle X-ray diffraction (WAXD) showed a slight shift of ZrP hkl planes and missing of some ZnG diffraction. According to thermogravimetry, there were free and physically anchored ZnG molecules into ZrP. Scanning electron microscopy showed that ZnG is disorderly distributed among lamellar ZrP platelets. Hydrogen low-field nuclear magnetic resonance (^{1}HLFNMR) revealed changes of α-ZrP molecular mobility. The material could be used potentially for drug control releasing.

Keywords Lamellar ZrP · Zinc gluconate · Intercalation · Thermal and structural properties · Relaxometry

Introduction

Ions and their salts play important roles in the biological processes of the human body. They have been used for several therapeutic purposes. For treatment of some disorders and illness, medicines based on sodium (I), magnesium (II), calcium (II), aluminum (III), and zinc (II) and other elements are available. Moreover, a non-toxic carrier for bioactive delivery is needed [1, 2].

Zinc gluconate is one of the most effective salts used as zinc supplement [3, 4]. Besides, administration of pharmacological doses of this element has been established as a treatment of several disorders/illness such as inflammatory acne [5], immune disturbances, common cold [6–8], dysgeusia (bad taste) [9], olfactory function therapy [10], and also for contraception/sterilization studies [11, 12].

The study of inorganic layered nanomaterials has been growing with potential for several biomedicine practical uses [13]. The application of such a nanovehicular system for delivering bioactive agents has been widely investigated. Nanosized drug delivery carriers have shown advantages for improving therapeutic efficiency due to the enhancement of permeation and reduction of side effects. Most studies showed that layered double hydroxide [2, 14] clays and tetravalent metal phosphate [15] such as zirconium phosphate (ZrP) [13, 16, 17] may be considered great drug carriers. One of the major advantages of these systems is their capacity to entrap high loads of bioactive species and protect them until they are released [13, 16].

In general, a chemical intercalation is required for the preparation of nanohybrid material as a host for control drug releasing. A quite simple chemical reaction is performed leading to attracting too much interest in many science fields. The chemical modification alters the physicochemical properties of the host material increasing its ability to accept the guest bioactive [18, 19].

Although having a large number of applications—catalyst, cation exchange, and others—the zirconium phosphate, α-Zr (HPO$_4$) 2H$_2$O, has been studied as a nanofiller for polymer nanocomposites [20–22]. The acid groups on the inner surface of its layers allow the direct intercalation of a variety of

✉ Luis C. Mendes
  lcmendes@ima.ufrj.br

[1] Instituto de Macromoléculas Professora Eloisa Mano, Universidade Federal do Rio de Janeiro, Avenida Horacio Macedo,2030, Centro de Tecnologia, Bloco J, Ilha do Fundão, Rio de Janeiro, RJ 21941-598, Brazil

Springer

substances, particularly basic substances such as alkylamines [23–26].

Alpha-ZrP has the capacity to incorporate several substances into its layer via direct ion exchange [13]. The intercalation of bioactive species into α-ZrP lamellae is a simple and easy ion exchange method allowing the preparation of very attractive nanocarriers for control drug delivery and other biotechnological applications [16, 17].

This study aimed to investigate the intercalation of zinc gluconate into α-zirconium phosphate lamellae. It was developed as a suitable and promising guest-host material to be used as a drug delivery system.

Experimental

Materials

Phosphoric acid (H_3PO_4) 85% P.A. and hydrated zirconium oxychloride ($ZrOCl_2.8H_2O$) P.A was purchased from Vetec, Brazil. Oligoetheramine (JeffamineTM M600 was provided by Sigma-Aldrich. Zinc gluconate was supplied by Diet Import S.A., Lisbon.

Synthesis of lamellar zirconium phosphate

Lamellar zirconium phosphate (α-ZrP) was synthesized by direct precipitation of 12 M solution of phosphoric acid and zirconium oxychloride at a Zr/P ratio equal to 18 using a three-neck flask. The reaction medium was maintained at 110 °C, during 24 h, under refluxing and stirring. After that, the reaction medium was centrifuged and washed successively with deionized water until the pH equaled to 5.0. Finally, the zirconium phosphate was frozen at − 80 °C during 24 h and lyophilized for 4 days [23, 27].The product was named as α-ZrP.

Intercalation of α-ZrP with zinc gluconate

The intercalation of the α-ZrP with zinc gluconate was conducted through mixing of ethanolic solution of phosphate and aqueous solution of zinc gluconate, at 25 °C, under magnetic stirring, during 24 h. Following, the reaction medium was filtered and washed with ethanol to ensure the removal of free zinc gluconate. Finally, the modified ZrP was dried in an oven at 80 °C. The product was named as ZrP-ZnG.

Differential scanning calorimetry

The differential scanning calorimetry (DSC) of the samples was performed using TA Instrument Q1000 calorimeter. Three thermal cycles were used. Firstly, the sample was heated from 20 to 250 °C, at a heating rate of 10 °C/min under nitrogen atmosphere and maintained for 2 min to remove the

thermal history. Then, the sample was cooled until 20 °C at a cooling rate of 100 °C/min. A second heating cycle was performed at the same conditions of the first one in order to compare the sample's thermal behavior.

Thermogravimetry/derivative thermogravimetry

Thermogravimetry/derivative thermogravimetry (TG/DTG) properties were evaluated using a TA Instrument Q500 thermogravimetric analyzer. The analysis was carried out from 30 to 700 °C, at 10 °C/min, using nitrogen as a carrying gas. Initial, maximum, and final degradation temperatures ($T_{initial}$, T_{max}, and T_{final}) were registered.

Wide-angle X-ray diffraction

The crystallographic patterns were registered by wide-angle X-ray diffraction (WAXD). The analysis was performed in a Rigaku equipment, model Ultima IV, using CuKα radiation with wavelength (15,418 Å), Ni filter, 40 kV, and 20 mA with 2θ between 2 and 50°. The filler interlayer spacing was evaluated by Bragg equation (Eq. 1),

$$n = 2\,d_{hkl}\,\text{sen}\,\theta; \qquad (1)$$

n diffraction order;
d_{hkl} interlayer spacing;
θ   diffraction angle.

Fourier-transform infrared spectroscopy

The analysis of chemical structure were performed with Perkin Elmer FTIR spectrometer, model Frontier. The spectra were taken from 400 to 4000 cm^{-1} with 50 scans and 4 cm^{-1} of resolution. The evaluation of the absorbance ratio between the bands at 3593 and 3511 cm^{-1} with invariable band at 661 cm^{-1} was proceeded in order to discuss on interaction of the ZrP and ZnG materials.

Field emission scanning electron microscopy

Field emission scanning electron microscopy was carried out in a Hitachi equipment, model S-4800 at 20 kV, vacuum and variable magnitude. The morphology, level of dispersion, and particle size were evaluated.

Hydrogen low-field nuclear magnetic resonance

The relaxometry analysis was performed applying hydrogen low-field nuclear magnetic resonance ([1]HLFNMR) in a Maran Ultra 23 low-field NMR equipment, in time intervals of 2 s and 40 points, at 30 °C. The results were expressed in terms of relaxation time (T_1H) and domain curves.
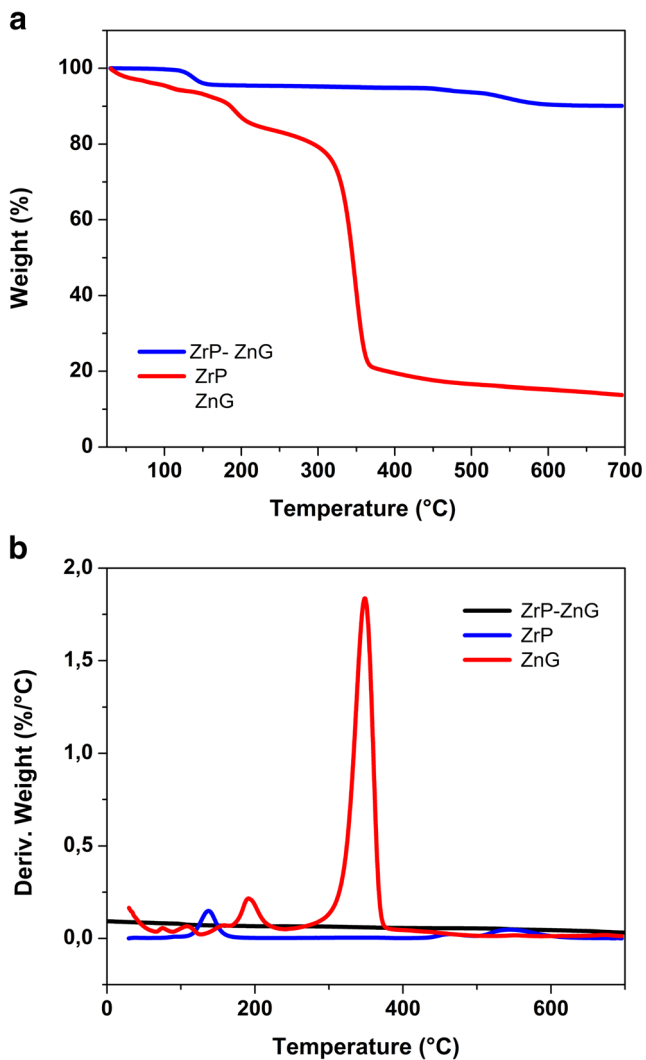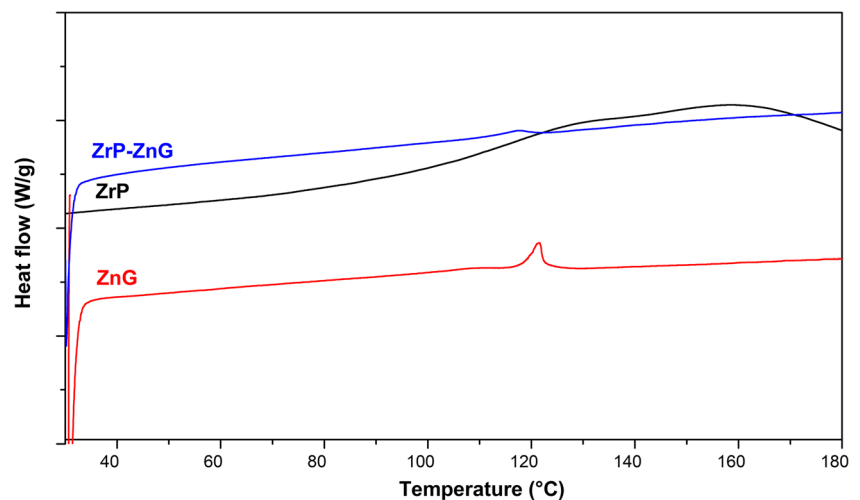
Fig. 1 TG (**a**) and DTG (**b**) curves of zinc gluconate (ZnG) and α-ZrP with and without zinc gluconate

Results and discussion

Thermogravimetry

Figure 1 shows the TG (a) and DTG (b) curves, respectively. For α-ZrP, three degradation steps were noticed. The first one occurred between 100 and 180 °C (maximum at 138 °C) being attributed to releasing of crystal/interlayer water. The intermediate step at 440–500 °C (maximum at 465 °C) was related to the dehydroxylation of P–OH groups. The third one around 500–600 °C (maximum at 541 °C) was associated with the chemical transformation of phosphate to pyrophosphate.

Zinc gluconate exhibited three weight loss steps below 250 °C and one between 300 and 350 °C indicating release of adsorbed water and thermal degradation of organic structure, respectively.

For ZrP-ZnG, three weight loss steps were detected and around 78% of zinc gluconate was incorporated. The first decay at about 140–220 °C (maximum at 189 °C) corresponded to the release of crystal/interlayer water. The second one between 275 and 375 °C (maximum at 319 °C) was attributed to the degradation of the free portion of zinc gluconate molecules into ZrP lamellae. The final degradation step appeared between 400 and 500 °C (maximum at 463 °C). It was deduced that some portion of ZnG molecules was physically anchored to the P–OH groups into lamellae and its thermal stability was increased.

Calorimetric properties

Figure 2 shows the second heating calorimetric curves of the samples. The ZrP curve did not present any modification along the temperature axis. ZnG exhibited an endothermic peak around 121 °C attributed to the crystal/interlayer water. For ZrP-ZnG, a slight alteration of the thermal curve around
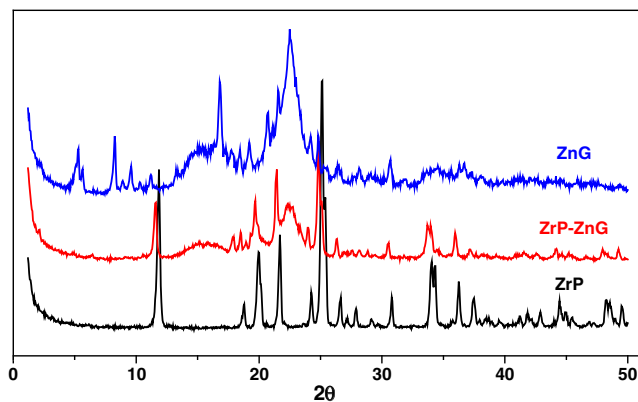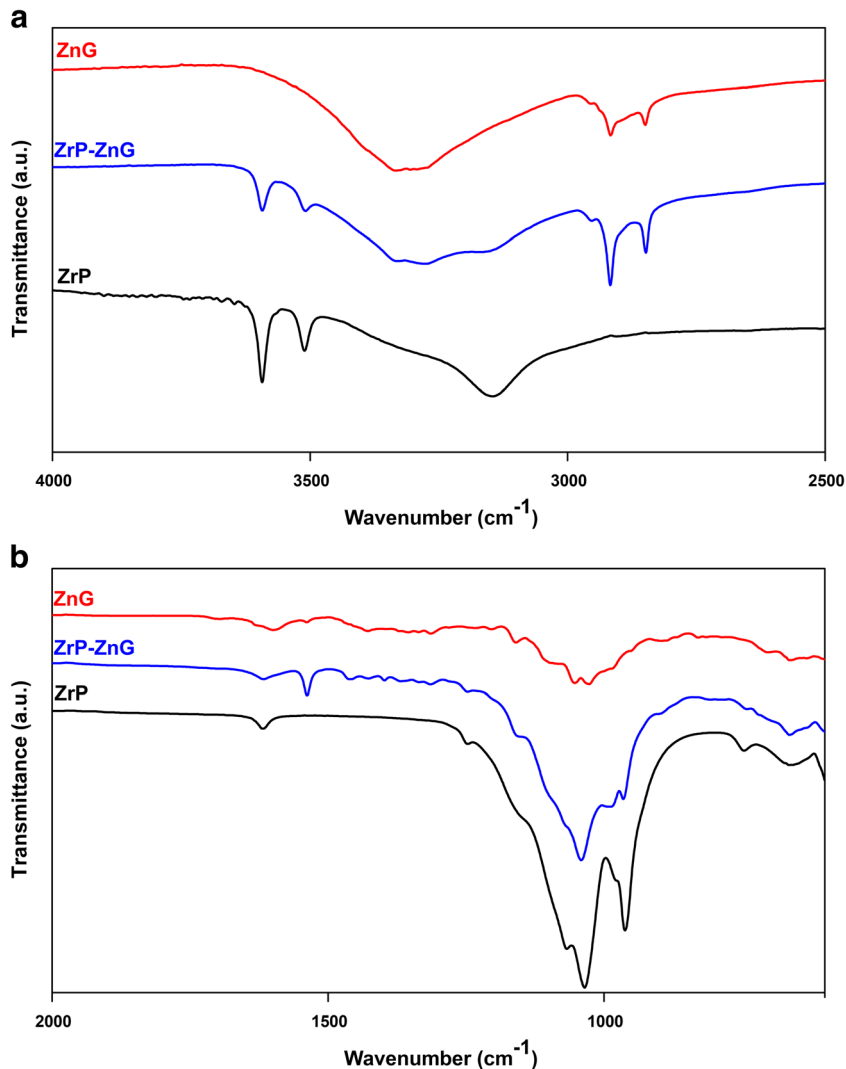
Fig. 2 Second heating calorimetric curves of zinc gluconate (ZnG) and ZrP with and without zinc gluconate

Fig. 3 WAXD patterns of zinc gluconate (ZnG) and α-ZrP with and without zinc gluconate

121 °C was also associated with the crystal/interlayer water. As the water remained, this could induce that zinc gluconate entered in the ZrP lamellae.

Wide-angle X-ray diffraction

Diffraction patterns of the samples are shown in Fig. 3. The 2θ angle of α-ZrP *hkl* plane appeared at 11.9° ($d_{spacing}$ equal to 7.4 Å) and are in agreement with Bestaoui et al. and Constantino et al. A series of diffraction angles was observed for zinc gluconate. The diffractogram has great similarity to the study reported by Ding et al. on preparation of zinc gluconate with different nanostructures. For ZrP-ZnG, significant changes were noticed. The diffraction angle of α-ZrP *hkl* plane was shifted to a lower value (11.5°) and $d_{spacing}$ slightly increased (7.7 Å). In some extent, platelet/platelet interactions were weakened. There were substantial changes of the zinc gluconate diffraction angles. All angles below 10° and that one around 17° disappeared. The angle at the vicinity of 22–23° drastically decreased. The changes in the zinc gluconate molecules arrangement evidenced its entrance into ZrP lamellae and that there was some physical interaction
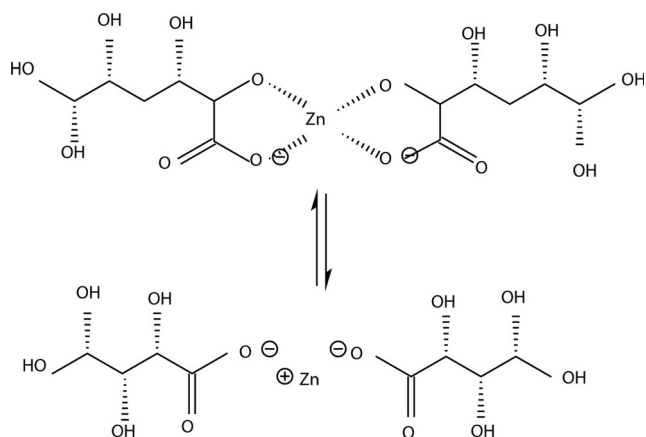
Fig. 4 Infrared spectra of zinc gluconate (ZnG) and α-ZrP with and without zinc gluconate: (**a**) 4000 to 2600 cm^{-1} (**b**) 2000 to 500 cm^{-1}

Fig. 5 Schematic representation of free and coordinate structures of carboxylate group in zinc gluconate

between host and guest entities. The results are in agreement with TG/DTG analysis.

Infrared spectroscopy

Figure 4 shows FTIR spectra of samples. For ZrP, absorption bands at 3595 and 3511 cm^{-1} were attributed to the stretching of free crystal/interlayer water. The absorption at 3153 cm^{-1} was recognized as hydrogen bonding of H–O–H and P–OH group. The absorption peak at 1617 cm^{-1} was also associated with the crystal/interlayer water. The 1075, 1050, and 968 cm^{-1} absorption bands were concerned to the PO$_4^{3-}$ vibrational modes while that around 594 cm^{-1} was considered as vibration of Zr–O bond [27, 28].

Zinc gluconate is an organic salt based on hydroxy-acid (Fig. 5). Above 3000 cm^{-1}, its spectrum presented a broad absorption band related to the hydrogen bonding of water and OH groups of zinc gluconate. Around 2927 and 2839 cm^{-1}, these two bands were assigned as the stretching of the C–H bond. Ishioka et al. in their study on vibrational spectra and structures of zinc acetate and zinc stearate pointed out that two absorption bands at 1500–1600 cm^{-1} were associated with the coordination mode of the carboxylate group. In this work, two bands at 1597 and 1541 cm^{-1} were also noticed. By analogy, they were assigned to the asymmetric stretching of the carboxylate group and related to the coordination mode of zinc and gluconate moieties. Another band related to the symmetrical stretching of the carboxylate anion was found around 1429 cm^{-1}. The bands at 1199, 1160, 1095,

Fig. 6 Illustration of the supposed interaction between the ZnG hydroxyl group and P–OH

Table 1 Absorbance ratio of specific bands to assessing interaction ZrP-ZnG

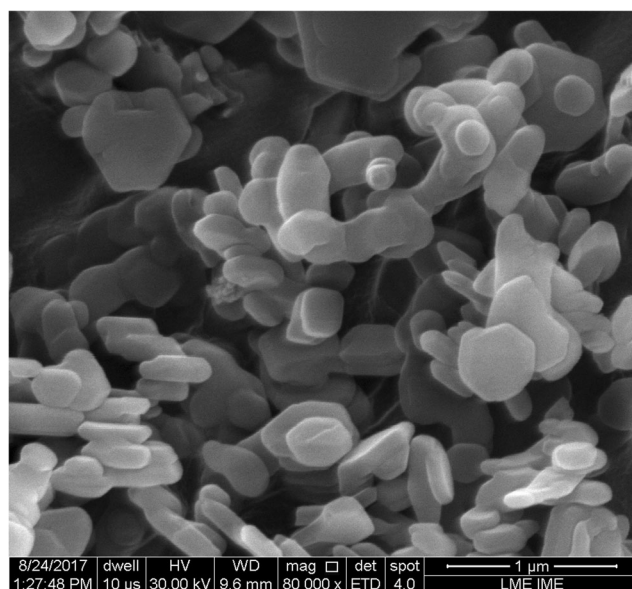| Band ratio	Absorbance ratio	
	ZrP	ZrP-ZnG
3593/661	0.91	0.45
3511/661	0.55	0.45

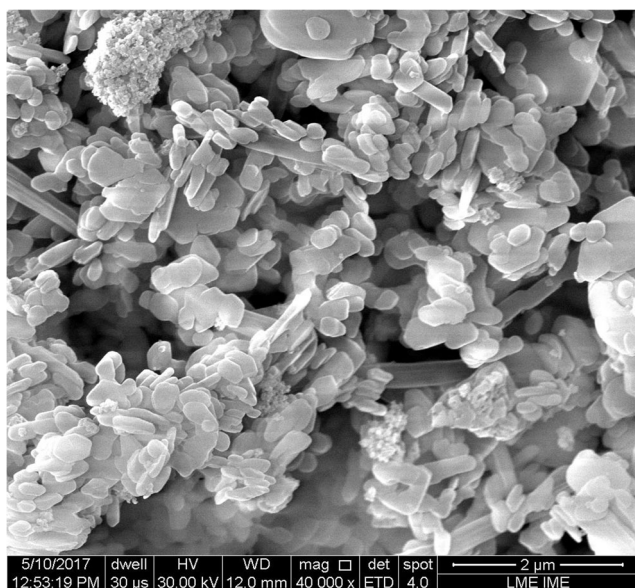**Fig. 7** SEM photomicrography of α-ZrP

Fig. 8 SEM photomicrography of ZrP-ZnG

1056, and 1025 cm^{-1} were concerned with the stretching of the C–O bond and asymmetric stretching of the O–C–C bond. Similarly as registered elsewhere, the bands at 896, 696, and 653 cm^{-1} were respectively associated with the vibrational deformation, angular deformation, and out-of-plane of carboxylate group [28, 29].

The IR spectrum of the ZrP-Zinc gluconate (ZrP-ZnG) material should be similar to the sum of the spectra of the lamellar ZrP except any chemical alteration of precursor materials happening after intercalation. Although, the bands at 3593 and 3511 cm^{-1} appeared their intensities decreased. In fact, the absorbance ratio between these bands with an invariable band at 661 cm^{-1} diminished (Table 1). This decrease was understood as the replacement of interlayer water by ZnG upon intercalation. This is an evidence of the interaction between ZrP/ZnG. The band around 3000 cm^{-1} presented a sharp

enlargement. Also, the presence of ZrP induced change in the carboxylate bands of the organic salt. The absorption bands at 1597 and 1541 cm^{-1} appeared as a doublet. The peak intensity of the band at 1541 cm^{-1} markedly increased. Once again, there was evidence of interaction between the P–OH group and ZnG hydroxyl group. In addition, the band at 968 cm^{-1} (P–OH vibration) showed marked reduction of peak intensity. These findings permit to emphasize two aspects. The ZnG molecules entered into α-ZrP lamellae. In some extent, the original ZnG coordinate mode was altered. It is reasonable to assume that the ZnG hydroxyl groups attached to the adjacent carbon of the carboxyl were associated with the P–OH group breaking the original zinc gluconate coordinate structure. This change is schematically illustrated in Fig. 6. The infrared results strongly suggest that the intercalation of the ZnG was successfully achieved.

Scanning electron microscopy

Figures 7 and 8 present the SEM images of the α-ZrP and ZrP-ZnG, respectively. For ZrP, a typical morphology for layered compounds is observed. Mixing of pseudo-hexagonal and rounded platelets was produced. The round edge of some of the sheets could be an indication that their crystallinity is still not very high as registered before [24]. For ZrP-ZnG, the image is similar to that of ZrP but aggregates of ZnG with different dimensions are disorderly distributed among the platelets and on the surface of the phosphate. Thus, the entrance of ZnG into host material was registered corroborating the assumption of the previous analyses.

Hydrogen low-field nuclear magnetic resonance

Either in a high field or in a low one, nuclear magnetic resonance (NMR) is an important tool for determining chemical composition and constitution, molecular mobility, and

Fig. 9 Domain curves and relaxation times of neat ZrP, ZnG, and ZrP-ZnG
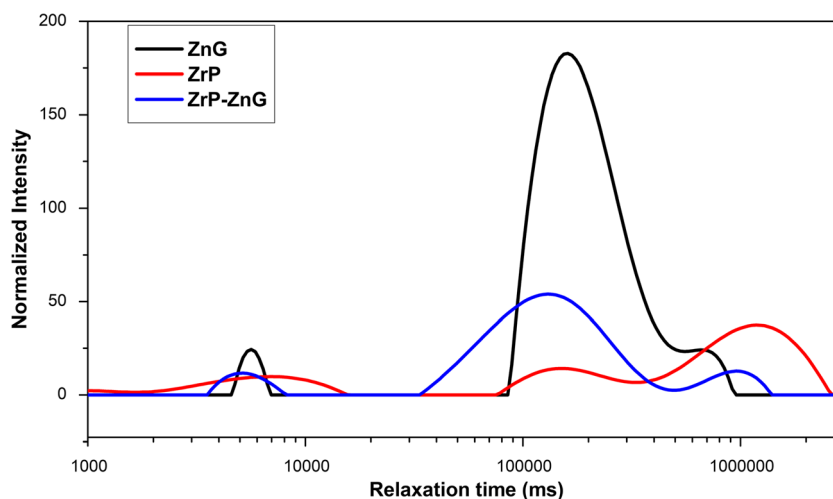
configuration of organic and inorganic compounds. Recently, hydrogen low-field NMR has been used for evaluating molecular structural organization and molecular dynamic in nanocomposites [30].

In this work, this technique was applied to assess the relaxometry of the materials. Figure 9 shows the domain curves of neat ZrP, ZnG and ZrP-ZnG, respectively. The relaxation domains of the ZrP showed two relaxation intervals. The first one lay around 7×10^2-2×10^4 ms while the second one at the vicinity of 8×10^4-3×10^6 ms, similar to domains found by Mendes et al. [22] and Lino et al. [31]. It is reasonable to consider that the hydrogen atoms attached to the water molecules must have a lower relaxation time. Based on it, it was supposed that the first relaxation interval represents the molecular mobility of free crystal/interlayer water molecules and those physically anchored to the P–OH group of the ZrP. The second interval of relaxation could be attributed to hydrogen relaxation of free P–OH, from the tip to the center of the ZrP lamellae. For ZnG, the relaxation curve presented a peak around 5×10^3–7×10^3 ms that was associated with the hydrogen relaxation of water molecules. Between 9×10^5 and 1×10^6 ms, a second peak was registered due to the hydrogen relaxation of the hydroxyl groups attached to the zinc gluconate. The ZrP-ZnG relaxation curve is unlike of that of neat ZrP. Three sharp relaxation peaks were noticed. The peak located at 2.5×10^3–7×10^3 ms was related to the hydrogen relaxation of the water molecules. The broad intermediate peak (3×10^4–5×10^5 ms) is merged from ZrP and ZnG ones, and it was understood as being the result of physical interaction of the P–OH groups and the hydroxyl groups attached to the ZnG. The peak at the highest relaxation times represented the free P–OH, where its low intensity was due to the occurrence of the partial interaction of P–OH and hydroxyl groups bonded in the chemical structure of ZnG.

Conclusions

The intercalation of zinc gluconate (ZnG) as a guest molecule into lamellar zirconium phosphate (α-ZrP) was performed. The phosphate was synthesized using phosphoric acid and zirconium oxychloride as precursors. In this study, the interaction and the entrance of the ZnG into the interlayer spacing was investigated. There were many evidences showing that ZnG was inserted into α-ZrP $d_{spacing}$. TG/DTG indicated that among ZrP platelets, there are free and physically anchored ZnG molecules. Diffractometry, infrared, and relaxometry analyses showed that there was the insertion of ZnG into ZrP lamellae and interaction between host and guest materials. Although several hydroxyl groups are attached in the guest chemical structure, they have very low basic strength, which decreases the probability of reaction with strong P–OH Brønsted acid groups in the ZrP interlayer region. The results

support that physical interaction predominated between ZrP and ZnG.

Compliance with ethical standards

Conflict of interest The authors declare that they have no conflict of interest.

References

1. Mjos KD, Orvig C (2014) Metallodrugs in medicinal inorganic chemistry. Chem Rev 114(8):4540–4563

2. Ghotbi MY, Hussein MZB, Yahaya AH, Rahman MZA (2009) LDH-intercalated D-gluconate: generation of a new food additive-inorganic nanohybrid compound. J Phys Chem Solids 70:948–954. https://doi.org/10.1016/j.jpcs.2009.05.007

3. Wegmuller R, Tay F, Zeder F, Benic M, Hurrell RF (2014) Zinc absorption by young adults from supplemental zinc citrate is comparable with that from zinc gluconate and higher than from zinc oxide1–3. J Nutr 144:132–136

4. Huifeng, Xu Z, Qianfengli, Wang X, Song Q (2015) One pot synthesis, characterization and mechanism of zinc glycinate monohydrate. International Conference on Applied Science and Engineering Innovation (ASEI 2015)

5. Gupta M, Mahajan VK, Mehta KS, Chauhan PS (2014) Zinc therapy in dermatology: a review. Dermatol Res Pract 2014:1–11. https://doi.org/10.1155/2014/709152

6. Eby GA, Davis DR, Halcomb WW (1984) Reduction in duration of common colds by zinc gluconate lozenges in a double-blind study. Antimicrob Agents Chemother 25(1):20–24

7. Tuner RB, Cetnarowski WE (2000) Effect of treatment with zinc gluconate or zinc acetate on experimental and natural colds. Clin Infect Dis 31:1202–1208

8. Science M, Johnstone J, Roth DE, Guyatt G, Loeb M (2012) Zinc for the treatment of the common cold: a systematic review and meta-analysis of randomized controlled trials. Can Med Assoc Licence 184(10):E551–E561

9. Heckmann SM, Hujoel P, Habiger S, Friess W, Wichmann M, Heckmann JG, Hummels T (2005) Zinc gluconate in the treatment of dysgeusia— a randomized clinical trial. J Dent Res 84(1):35–38

10. Duncan-Lewis CA, Lukman RL, Banks RK (2011) Effects of zinc gluconate and 2 other divalent cationic compounds on olfactory function in mice. Comp Med 61(4):361–365

11. Vannucchi CI, Angrimani DSR, Eyherabide AR, Mazzei CP, Lucio CF, Maiorka PC, Silva LCG, Nichi M (2015) Effects of intratesticular administration of zinc gluconate and dimethyl sulfoxide on clinical, endocrinological, and reproductive parameters in dogs. Theriogenology 84:1103–1110

12. Araujo-Lima CF, Nunes RJM, Carpes RM, Aiub CAF, Felzenszwalb I (2017) Pharmacokinetic and toxicological evaluation of a zinc gluconate-based chemical sterilant using in vitro and in silico approaches. Biomed Res Int 2017:1–8. https://doi.org/10.1155/2017/5746768

13. Dias A, Saxena V, Gonzalez J, David A, Casañas B, Carpenter C, Batteas JD, Cólon JL, Clearfield A, Hussain MD (2012) Zirconium phosphate nano-platelets: a novel platform for drug delivery in

cancer therapy. Chem Commun 48:1754–1756. http://pubs.rsc.org. https://doi.org/10.1039/C2CC16218K

14. Hussein MZ, Rahman NSSA, Sarijo SH, Zainal Z (2012) Herbicide-intercalated zinc layered hydroxide nanohybrid for a dual-guest controlled release formulation. Int J Mol Sci 13:7328–7342. https://doi.org/10.3390/ijms13067328

15. Pourbaghi-Masuleh M, Hosseini V (2013) Amorphous calcium phosphate nanoparticles could function as a novel cancer therapeutic agent by employing a suitable targeted drug delivery platform. Nanoscale Res Lett 8:449–455 http://www.nanoscalereslett.com/content/8/1/449

16. Saxena V, Diaz A, Clearfield A, Batteas JD, Hussain MD (2013) Zirconium phosphate nanoplatelets: a biocompatible nanomaterial for drug delivery to cancer†. Nano 5:2328–2336. www.rsc.org/nanoscale/. https://doi.org/10.1039/c3nr34242e

17. González GL, Ortíz M, Hérnandez C, Cában J, Rodriguez A, Cólon JL, Báez A (2015) Zirconium phosphate nanoplatelet potential for anticancer drug delivery applications. J Nanosci Nanotechnol 15:1–13. www.aspbs.com/jnn/. https://doi.org/10.1166/jnn.2015.11608

18. Casanas-Montes B, Dias A, Barbosa C, Ramos C, Collazo C, Melendez E, Quefelec C, Fayon F, Clearfield A, Bujoli B, Cólon JL (2015) Molybdocene dichloride intercalation into zirconium phosphate nanoparticles. J Organomet Chem 791:34–40

19. Gonzaléz-Villegas J, Kan Y, Bakhmutov VL, García-Vargas A, Martínez M, Clearfield A, Cólon JL (2017) Poly(ethylene glycol)-modified zirconium phosphate nanoplatelets for improved doxorubicin delivery. Inorg Chim Acta 468:270–279. https://doi.org/10.1016/j.ica.2017.05.057

20. Mariano DM, Freitas DFS, Mendes LC (2017) Nanocomposite of polypropylene/ octadecylamine lamellar-zirconium phosphate: influence of nanofiller and screw speed. J Compos Mater 52:1–11. https://doi.org/10.1177/0021998317713832 journals.sagepub.com/home/jcm

21. Mendes LC, Silva DF, Lino AS, Araujo LJF (2014) Zirconium phosphate organically intercalated/exfoliated with long chain amine. J Therm Anal Calorim 118(3):1461–1469. https://doi.org/10.1007/s10973-014-4056-0.

22. Mendes LC, Silva DF, Lino AS (2012) Linear low-density polyethylene and zirconium phosphate nanocomposites: evidence from thermal, thermo-mechanical, morphological and low-field nuclear magnetic resonance techniques. J Nanosci Nanotechnol 12(12):8867–8873. https://doi.org/10.1166/jnn.2012.6718

23. Brandao LS, Mendes LC, Medeiros ME, Sirelli L, Dias ML (2006) Thermal and mechanical properties of poly(ethylene terephthalate)/lamellar zirconium phosphate nanocomposites. J Appl Polym Sci 102(4):3868–3876. https://doi.org/10.1002/app.24096.18

24. Sun L, Boo WJ, Browning RL, Sue H, Clearfield A (2005) Effect of crystallinity on the intercalation of monoamine in r-zirconium phosphate layer structure. Chem Mater 17:5606–5609 http://pubs.acs.org/doi/abs/10.1021/cm051160i

25. Alberti G, Costantino U, Allulli S, Tomassini N (1978) Crystalline Zr(R-PO3) 2 and Zr(R-OPO3) 2 compounds: a new class of materials having layered structure of the zirconium phosphate type. J Inorg Nucl Chem 40(6):1113–1117. https://doi.org/10.1016/0022-1902(78)80520-X.16

26. Clearfield A, Smith GD (1969) The crystallography and structure of zirconium bis(monohydrogen orthophosphate) monohydrate. Inorg Chem 8(3):431–436. https://doi.org/10.1021/ic50073a005.17

27. Hajipour AR, Karimi H (2014) Synthesis and characterization of hexagonal zirconium phosphate nanoparticles. Mater Lett 116:356–358. https://doi.org/10.1016/j.matlet.2013.11.049

28. Prestch E. (2009). Structural determination of organic compounds Fouth, Revised and enlarged edition. Springer

29. Ishioka T, Shibata Y, Takahashi M, Kanesaka I (1998) Vibrational spectra and structures of zinc carboxylates II. Anhydrous zinc acetate and zinc stearate. Spectrochim Acta A 54:1811–1818

30. Tavares MIB, Rodrigues T, Soares I, Moreira A, Ferreira A (2009) The use of solid state NMR to characterize high density polyethylene/organoclay nanocomposites. Chem Chem Technol 3(3):187–190 http://old.lp.edu.ua/fileadmin/ICCT/journal/Vol.3/Num.3/05.pdf

31. Lino AS, Mendes LC, Silva DF, Malm O (2015) High density polyethylene and zirconium phosphate nanocomposites. Polímeros 25(5):477–482 https://www.researchgate.net/publication/286924711